https://doi.org/10.20965/jdr.2023.p0308

Paper:

Seismicity Based Maximum Magnitude Estimation of Subduction Earthquakes in Peru

Juan Carlos Tarazona*,†, Zenon Aguilar*, Nelson Pulido, Carlos Gonzales*, Fernando Lazares*, and Hiroe Miyake*****

*Japan Peru Center for Earthquake Engineering Research and Disaster Mitigation (CISMID), National University of Engineering (UNI)
Av. Tupac Amaru 1150, Lima 15333, Peru
†Corresponding author, E-mail: jtarazona@uni.pe
**National Research Institute for Earth Science and Disaster Resilience (NIED), Tsukuba, Japan
***Earthquake Research Institute, The University of Tokyo, Tokyo, Japan
[Received January 8, 2023; accepted April 6, 2023]

In seismic design, intensity parameters that represent seismic demand are commonly used. A probabilistic seismic hazard assessment is an accurate way of assessing seismic demand, based on a set of parameters that represent the seismicity of a region. However, because some regions lack sufficient information, the selection of these parameters can be controversial. In Peru, selecting a maximum earthquake magnitude (M_{max}) for regional seismic hazard assessments has proven to be a challenging task due to the limited available information concerning of large-magnitude events. This study evaluated the M_{max} for subduction earthquakes using scaling relationships, empirical evidence, and the extreme value statistics (Kijko and Bayesian) approach. The seismic catalog was updated to February 2022 and divided into 19 subduction seismic sources (5 interface and 14 intraslab). The results showed that the obtained M_{max} are within the range of M_w 8.7–9.0 for the interface and M_w 7.6–8.1 for the intraslab sources, which unlike the M_{max} values established in previous regional seismic hazard assessments, are more consistent with the historical and instrumental seismicity and rupture models.

Keywords: maximum magnitude, subduction earthquakes, seismogenic sources, interface and intraslab earthquakes, seismic zonation

1. Introduction

The probabilistic seismic hazard assessment (PSHA) is commonly used for estimating the ground motion intensity (e.g., peak ground acceleration (PGA), peak ground velocity (PGV), and Arias intensity), which is used for the seismic analysis and structural design. An essential aspect of estimating the seismic hazard of a site is the correct representation of local seismicity, represented by seismogenic sources that group the earthquakes according to their focal mechanism and spatial distribution. For PSHA, one of the necessary inputs is seismic recurrence, a parameter that requires ascertaining the maximum magnitude (M_{max}) associated with each source. The value of M_{max} significantly influences the PSHA results and is accentuated as the return period of the scenario earthquake increases [1]. Traditionally, M_{max} is based on historical information; however, there are places where this type of data is scarce or non-existent, such as northern Peru.

Several seismogenic source models have evolved in Peru [2–6] and been employed in regional seismic hazard studies in recent years. However, different sources and their respective recurrence parameters (e.g., M_{max}) create discrepancies between the values reported in each study for the same location. Although it can be argued that the recurrence parameters vary owing to the different seismic source models, the M_{max} adopted in studies varies significantly. One of the main problems encountered in the estimates of M_{max} proposed in these studies is that they present substantial differences with respect to historical catalogs [7–9], physical studies [10–12], and recently recorded events, such as the 2019 Lagunas earthquake, which registered a magnitude of M_w 8.0 [13].

While several methods for estimating M_{max} of earthquakes have been proposed in the literature, information on large earthquake magnitudes remains scarce. For instance, the empirical approach consists of adding a variable or constant increment to the largest observed magnitude (M_{max}^{obs}) [14]; the statistical extreme value approach or Kijko's method [15, 16], based on the observed seismicity and the M_{max}^{obs}, determines M_{max}; the Bayesian approach [17, 18], multiplies an a priori probability distribution by a likelihood function, forming a posterior probability distribution for M_{max}; and the approach of scaling relationships [19, 20] involves using scaling relationships from comparable tectonic settings to estimate M_{max} based on source rupture characteristics.

This study aims to determine the M_{max} for interface and intraslab subduction sources in Peru from an updated seismic catalog using the aforementioned methods used in the PSHA of Peru.

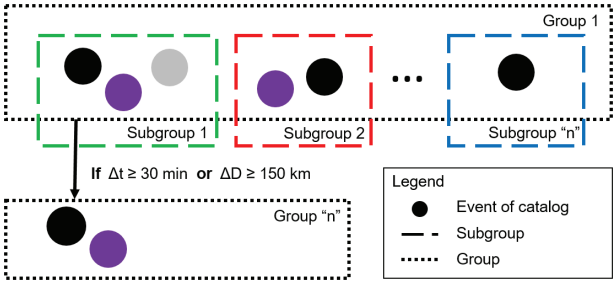

Fig. 1. Event grouping scheme for duplicate elimination.

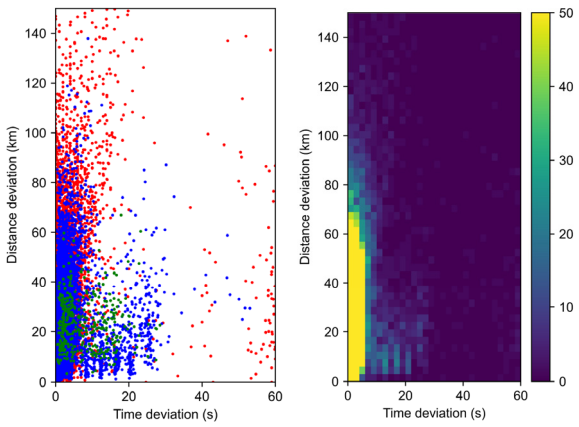

Fig. 2. Graph of average temporal and spatial variation of each subgroup. (a) Red represents a group consisting of an N° of catalogs ≤ 3, blue a $3 < \text{N}° < 7$, and green an N° ≥ 7. (b) The bivariate density distribution: the heat map represents the number of groups.

2. Seismic Catalog

The study area lies between the parallels of 7°N and 28°S and the meridians of 63°W and 86°W. The seismic catalog for the study area was compiled from events reported in nine seismic catalogs published by the Geophysical Institute of Peru (IGP), the International Seismological Center (ISC, ISC-REV, and ISC-GEM catalogs), the Centroid Moment Tensor (CMT), the United States Geological Survey (USGS), the National Oceanic and Atmospheric Administration (NOAA), the South America Risk Assessment (SARA), and the Northern California Earthquake Data Center (NCEDC). Data updated on February 28, 2022 were collected. Instrumental seismic events of $M_w \geq 4.0$ and historical events reported in paleoseismic and macroseismic studies [7–9] within the aforementioned spatial window were selected. Events reported at different magnitude scales were converted to M_w using the expressions proposed by Scordilis [21].

2.1. Elimination of Duplicate Events

To eliminate duplicate events (i.e., events reported by two or more agencies), we first created groups of events located within 150 km of each other and whose time of origin was less than 30 min apart. Subgroups were then created based on the maximum number of events reported in the same catalog. Each subgroups included an event from the predominant catalog and events reported in the other catalogs that were spatially and temporally close to that event, as well as within a magnitude difference of less than one degree, as shown in **Fig. 1**. Temporal and spatial variation was calculated as the average of the difference in the origin times of each event and the average of the distances at which the events of each subgroup were located one by one, respectively (**Fig. 2**).

As shown in **Fig. 2**, a smaller temporal and spatial variation between events indicates that the data reported in different catalogs correspond to the same event. Subgroups with a temporal variation of less than 40 s and a spatial variation of less than 100 km were considered duplicates. Therefore, a single representative event was selected for each subgroup, prioritizing, in descending order of importance, the events containing the magnitude types M_w, M_S, mb, M_L, and others, as well as the catalogs in which they were reported. Similarly, a second priority order was established based on the agencies of the seismic catalogs, which were differentiated into two periods. For earthquakes occurring before 1960, the IGP was considered the first priority because it was a national agency. The compiled catalog of the SARA project was included in second place, as the IGP has updated magnitudes that may differ from SARA's databases. Additionally, the compilation of large events, including NOAA's catalog, was included in third place to complement historical events from other regions. The remaining catalogs were assigned the same priority. Second, for events after 1960, the priority was assigned to highest priority was assigned to the CMT catalog, as it offers additional information such as the type of focal mechanism of the event, which is of great interest for this research. The next one in the priority list is the IGP, which is a national agency with a large seismic network in Peru. Thereafter, priority was given to more regional catalogs, such as the ISC-GEM and ISC-REV, followed by the SARA project catalog, which was updated only until 2013. Finally, the remaining catalogs were assigned the same priority.

The selection process was complemented with a manual review of events with magnitudes greater than M_w 7.0 was performed. The results indicated that the USGS seismic catalog contained some events whose origin times differed between 10 and 20 h from those reported for the other catalogs, and these were removed from the database. **Fig. 3** shows the event content of the catalog without duplicates.

2.2. Tectonic Classification of Seismicity

The events were classified according to the criteria established in [22] using the USGS Slab2.0 subduction model [23] and the LITHO1.0 crustal model [24]. The classification routine categorizes seismic catalogs into interface, intraslab, crustal, and unclassified categories. A 10 km downward buffer zone relative to the Moho discontinuity was used to classify the crustal events. Subduction

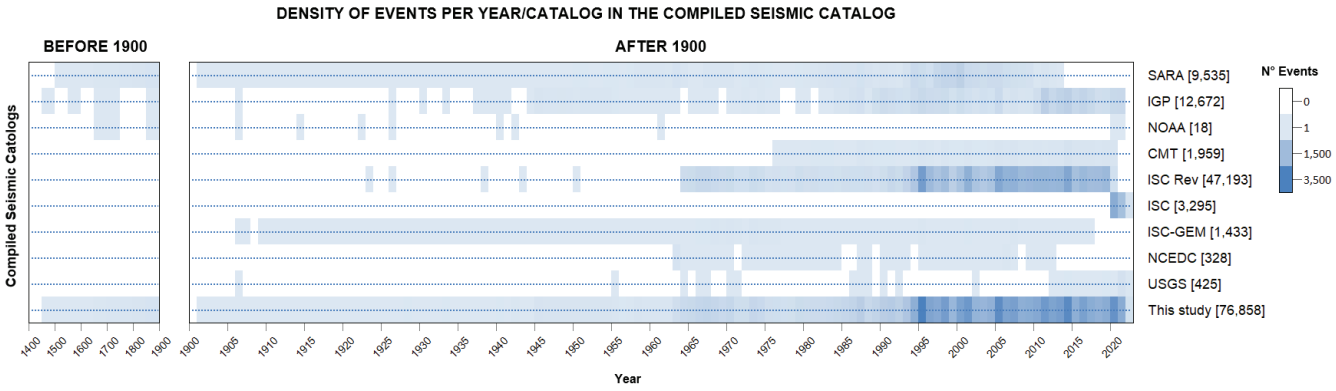

Fig. 3. Density of events per year/catalog in the compiled seismic catalog with $M_w \geq 4$. The color density indicates earthquake frequency for events after 1900, and every 50 years before.

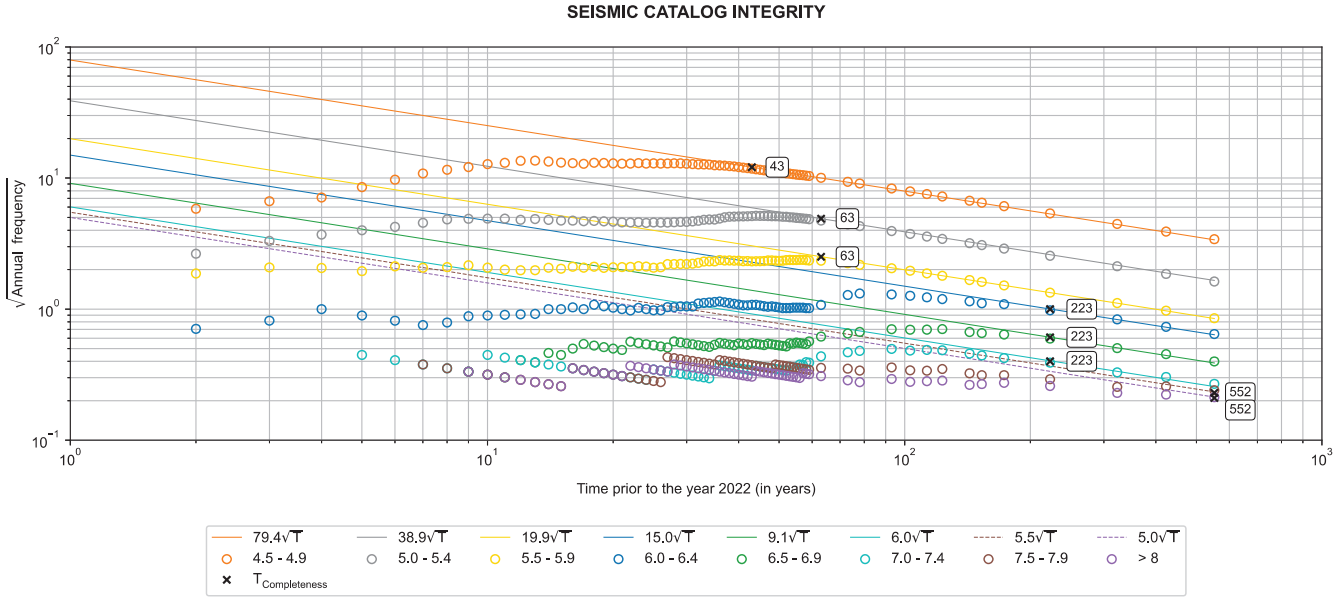

Fig. 4. Graph of integrity analysis using the Stepp's method [28].

events were divided into interface and intraslab events considering a boundary at a depth of 60 km. To classify intraslab events, buffers of 35 km above and 100 km below Slab2.0 were used, whereas a buffer of 20 km from both sides of Slab2.0 was used for interface events. The interface was ranked as intraslab or crustal for events that occurred in more than one seismogenic zone. Those events that do not belong to any of the mentioned seismogenic zones were considered "unclassified."

Large-magnitude events located at the boundary of the interface and intraslab mechanisms were reviewed in the CMT catalog [25]. The interface and intraslab mechanisms were assigned to events with reverse faults and normal faults, respectively. Events of $M_w \geq 6.0$ were reviewed manually to verify their location and any other available information that could imply a change in their classification. The seismic catalog did not consider instrumental events with $M_w < 6.0$ with undefined or default depths. Historical events without depth data were assigned manually.

2.3. Seismic Catalog Declustering and Completeness Analysis

The declustering process involved eliminating seismic events cataloged as aftershocks and foreshocks using the methodologies proposed by Gardner and Knopoff [26]. The time windows proposed by Uhrhammer [27] were used, and catalog integrity analysis was performed using the method proposed by Stepp [28] (**Fig. 4**).

The results show that the elaborated catalog is complete since 1980 for $M_w < 5.0$, since 1960 for $5.0 \leq M_w < 6.0$, since 1800 for $6.0 \leq M_w < 7.5$, and since 1471 for $M_w \geq 7.5$. Likewise, when considering only the interface earthquakes of the catalog, completeness was obtained from 1960 for $5.0 \leq M_w < 6.0$, from 1900 for $6.0 \leq M_w < 7.5$, and from 1513 for $M_w \geq 7.5$. Similarly, completeness was obtained for intraslab earthquakes since 1960 for $5.0 \leq M_w < 6.0$ and since 1900 for $M_w \geq 6.0$.

3. Methods for the Estimation of Maximum Magnitudes

3.1. Empirical Approach

The empirical approach involves adding a variable or constant increment to $M_{\max}^{\text{obs}}$ [14]. This increment should be sufficiently large to provide protection against earthquakes with magnitudes greater than $M_{\max}^{\text{obs}}$. In addition, as $M_{\max}^{\text{obs}}$ increases, a smaller increment is typically assigned to reach the maximum value expected for the source mechanism [14].

3.2. Kijko's Method

The Kijko's method [16] follows an approach based on extreme value statistics to estimate the $M_{\max}$ ($M_{\max}^{\text{K}}$). This method requires a declustered seismic catalog to be completed above a threshold magnitude (M_0) with a certain number of events (n). The $M_{\max}$ is calculated recursively using Eqs. (1) and (2). In Eq. (1), a magnitude increment (Δ) is added to the $M_{\max}^{\text{obs}}$. The value of Δ (Eq. (2)) is a function of β, a counterpart of b in the Gutenberg–Richter relation, $M_{\max}$, M_0, and n [15, 16]. This method estimates $M_{\max}$ more accurately for n values of 50 and 150 when the range of magnitudes ($M_{\max} - M_0$) does not exceed two and three, respectively [16].

$$M_{\max}^{\text{K}} = M_{\max}^{\text{obs}} + \int_{M_0}^{M_{\max}} F_{M_n}(m)dm = M_{\max}^{\text{obs}} + \Delta, \quad . \quad (1)$$

$$\Delta = \int_{M_0}^{M_{\max}^{\text{K}}} \left[\frac{1 - \exp\left[-\beta(m - M_0)\right]}{1 - \exp\left[-\beta(M_{\max}^{\text{obs}} - M_0)\right]} \right]^n dm. \quad (2)$$

3.3. Bayesian Method

In regions with low seismicity, the limited availability of data makes it difficult to estimate $M_{\max}^{\text{K}}$ [16]. This is because the observed value of $M_{\max}^{\text{obs}}$ is generally lower than the probable value of $M_{\max}$ or a low value of n. If there is a large $M_{\max}^{\text{obs}}$ and a low value of n, the resulting Δ would be too large, leading to an unrealistic estimation of $M_{\max}$. Accordingly, a Bayesian approach was developed [17,18]. This approach is based on the ergodic assumption and regional databases, and consists of three steps.

First, the tectonic environment of the study region was classified and the statistics of $M_{\max}^{\text{obs}}$ from similar regions were collected to obtain a distribution function with the mean of $M_{\max}^{\text{obs}}$ (μ_{regional}) and its standard deviation (σ_{regional}).

In the second step, the prior distribution (μ_{prior} and σ_{prior}) are obtained by modifying the μ_{analog} and σ_{analog} distributions with the cumulative distribution function of Eq. (3) [29].

$$F\left(M_{\max}^{\text{obs}}\right) = \left[\frac{1 - \exp\left\{-\beta\left(M_{\max}^{\text{obs}} - M_0\right)\right\}}{1 - \exp\left\{-\beta\left(M_{\max} - M_0\right)\right\}} \right]^n, \quad \text{for } M_0 \le M_{\max}^{\text{obs}} \le M_{\max}. \quad (3)$$

Finally, the prior distribution is updated using the likelihood function given by Eq. (4), where $\Delta_M = (M_{\max} - M_0)$, resulting in the expected distribution of $M_{\max}$ using the Bayesian approach ($M_{\max}^{\text{B}}$).

$$\mathscr{L}(M_{\max}|m,\beta) = \begin{cases} 0, & m < M_{\max}^{\text{obs}} \\ \left(\dfrac{1}{1 - \exp[-\beta\Delta_M]} \right)^n, & m \ge M_{\max}^{\text{obs}} \end{cases} \quad . \quad (4)$$

3.4. Scaling Relationships for Seismogenic Sources

Scaling relations allow the determination of rupture geometry from the magnitude of a seismic event. Similarly, $M_{\max}$ ($M_{\max}^{\text{R-S}}$) can be estimated from the geometry of a characterized maximum rupture, making it possible to estimate the $M_{\max}$ ($M_{\max}^{\text{R-S}}$). A hypothetical rupture in the seismic source area (A) can be used for interface earthquakes. According to [20], $M_{\max}$ estimates are often limited by the entire subduction slab thickness (W), which can be obtained from Slab2.0 [23]. However, assuming that a complete rupture of the thickness does not usually represent the typical characteristics of the rupture areas of the largest events, a factor can be used with respect to W to estimate a credible rupture thickness, and thus obtain a reasonable estimation of $M_{\max}$. Scaling relationships applicable to subduction mechanisms are presented in [19, 20]. However, even when the source geometry can be correctly characterized and is consistent with the tectonic regime, because the scaling relations are created from global databases, there are uncertainties in the $M_{\max}$ obtained using this method [1].

4. Estimation of the Maximum Magnitude

4.1. Zoning and Delimitation of Seismogenic Sources

First, a grid of points at 0.2° latitude and longitude was created over the study area and projected onto Slab2.0 [23]. Events with the same focal mechanism (interface or intraslab) were grouped into cylindrical volumes with radii of 150, 200, 250, and 300 km and axes at each point of the grid. Recurrence parameters (e.g., β, n, and $M_{\max}^{\text{obs}}$) were then obtained for the earthquakes enclosed in the section of each volume, and $M_{\max}^{\text{K}}$ was calculated from Eqs. (1) and (2). When the value of n was very low, the values of $M_{\max}^{\text{K}}$ were too high; therefore, $M_{\max}^{\text{B}}$ was used to estimate a more realistic value. $M_{\max}^{\text{B}}$ was calculated using Eq. (4) with the same discretization and recurrence parameters defined for the calculation of $M_{\max}^{\text{K}}$. The calculation of $M_{\max}^{\text{B}}$ requires Eq. (3) to establish a prior distribution of $M_{\max}^{\text{obs}}$ in the region. It was necessary to first assume a normal distribution given by $\mu_{\text{prior}} = 8.0$, $\sigma_{\text{prior}} = 0.2$ and $\mu_{\text{prior}} = 9.0$, $\sigma_{\text{prior}} = 0.2$ for intraslab and interface events, respectively.

In the second step, the value of $M_{\max}$ was defined as the smaller value of $M_{\max}^{\text{K}}$ and $M_{\max}^{\text{B}}$ was determined for each point on the grid. Then the values of $M_{\max}$ in the region were plotted, and an initial zoning was delineated,

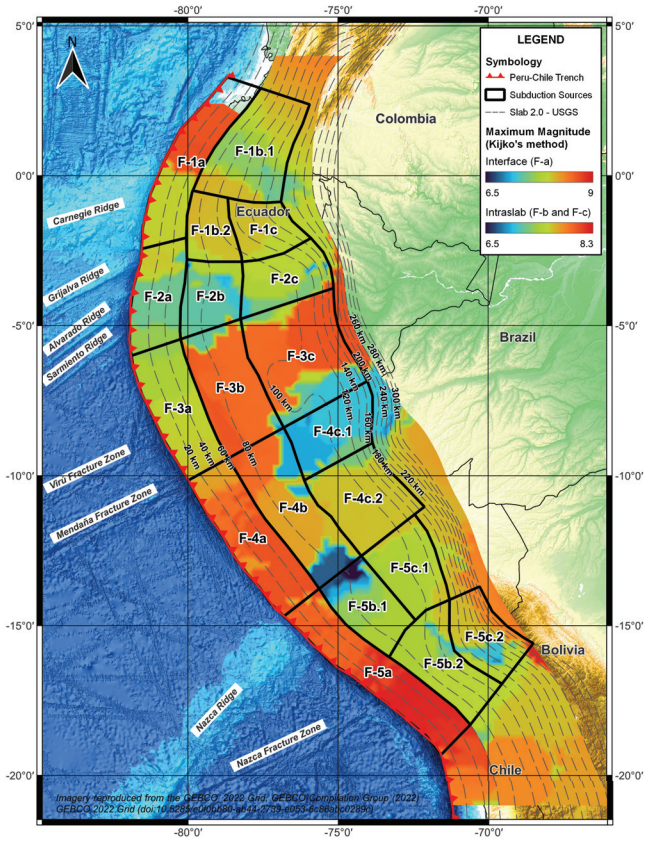

Fig. 5. Distribution of maximum magnitudes for interface and intraslab earthquakes using the Kijko's method [16] and delimitation of seismogenic sources.

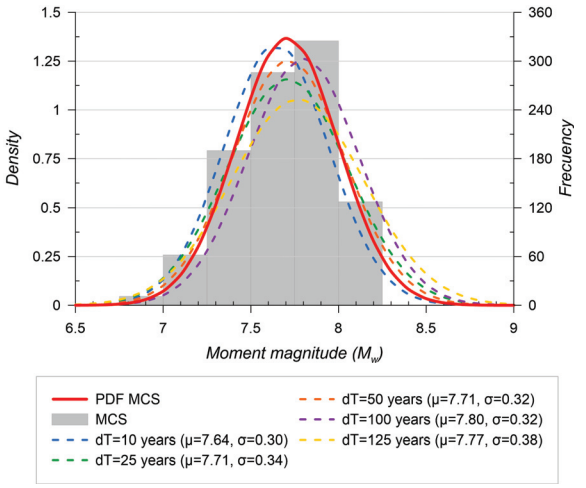

Fig. 6. Distribution of $M_{\max}^{\text{obs}}$ simulated samples by the MCS method and samples generated from time windows. Dashed lines correspond to the standard distribution model from the time windows. The solid line corresponds to the standard distribution model generated from the MCS samples, shown in gray.

outlining zones with similar $M_{\max}$ extrapolations and tectonic features of the region (**Fig. 5**). Next, the values of $M_{\max}$ were recalculated by updating the values of μ_{prior} and σ_{prior} from the first step using Eq. (3), which yielded similar values. Finally, these $M_{\max}$ values were used to define five seismic zones for the interface mechanism and 14 intraslab zones, as shown in **Fig. 5**.

The interface sources were delimited from the trace of the trench to a depth of 60 km from Slab2.0. Similarly, these sources were sectorized considering the Arica Deflection (19°S), the Nazca Ridge (15°S), and the Mendaña Fracture (10°S). The northern area of the Mendaña Fracture was divided into three seismogenic sources, showing that the central source (F-2a) had a lower $M_{\max}$, possibly due to the influence of the Sarmiento, Alvarado, and Grijalva ridges, which strike directly against it.

The intraslab sources were delineated from a depth of 60 km to a mean depth of 180 km. These sources were sectioned from the Arica Deflection (19°S), Nazca Fracture (17.5°S), Nazca Ridge (15°S), Mendaña Fracture (10°S), Sarmiento Ridge (6.5°S), Grijalva Gidge (3°S), and Carnegie Ridge (1°S). Source F-4c was then split into two sub-sources because source F-4c.1 had a lower extrapolation of $M_{\max}$ and coincided with the distortion of Slab2.0. Furthermore, source F-5c.2 was added from a depth of 140–300 km between the Arica Deflection (19°S) and the Nazca Fracture (17.5°S) to gather the large seismic activity recorded in this area.

Once the seismic sources were delineated, $M_{\max}$ was updated by estimating the μ_{regional} and σ_{regional} distributions using the criteria described in [29]. As described in [29], Monte Carlo simulations (MCS) were performed using the annual occurrence rates of each magnitude (λ_M) from the seismic catalog. For this purpose, a total of 1,000 simulations were considered for four different sample sizes (5, 30, 100, and 200), and only events with magnitudes greater than M_{w} 7.0 and 6.0 for interface and intraslab earthquakes, respectively, were considered. The distributions for both the interface and intraslab earthquakes remained consistent regardless of the sample size used in the MCS. Therefore, the probability density function (PDF) MCS obtained from 1,000 simulations with a sample size of 100 events was used.

For intraslab events, a PDF MCS was obtained with $\mu_{\text{regional}} = 7.71$ and $\sigma_{\text{regional}} = 0.29$, which was compared with distributions obtained from different time windows of the intraslab seismic catalog since 1400 CE, considering only events larger than M_{w} 7.0. Both analyses showed similar results (**Fig. 6**), therefore, we decided to use the PDF MCS as the representative $M_{\max}^{\text{obs}}$ distribution for the analog regions.

Similarly, the PDF MCS was estimated for interface events with $\mu_{\text{regional}} = 8.81$ and $\sigma_{\text{regional}} = 0.36$. However, because the method requires the inclusion of similar regional databases, earthquakes from the Chilean region located at latitudes below the cutoff of the seismic catalog (28°S) were added. These earthquakes included Chile's largest historical interface events [30], such as the Valdivia Earthquake (M_{w} 9.5) considered the largest recorded earthquake in the world and the Arica Earthquake of 1868 (M_{w} 8.8), which is the largest interface earthquake ever recorded in Peru.

Next, the a priori distributions of each seismic source were calculated using Eq. (3) and the distribution of $M_{\max}^{\text{obs}}$ obtained from the MCS. The most unfavorable a priori distribution of each focal mechanism was selected to replace the initially assumed a priori distribution (i.e., global distribution). The selected a priori distributions for the intraslab and interface mechanisms corresponded to seismic F-3c.1 and F-5a, respectively. The distribution of F-3c.1 ($\mu_{\text{prior}} = 7.91$, $\sigma\mu_{\text{prior}} = 0.18$) was obtained from $\beta = 0.841$, $M_{\max}^{\text{obs}} = 8.0$, and $N[M \geq 6.0] = 23$, where the correction for the number of earthquakes greater than $M_0(N_C(M_0))$ was calculated using Eq. (5) [29] and considering a seismic catalog completeness time for $M_{\max}^{\text{obs}}$ ($T_C(M_{\max}^{\text{obs}})$) of 552 years. Similarly, the distribution of F-5a ($\mu_{\text{prior}} = 9.16$, $\sigma\mu_{\text{prior}} = 0.21$) was estimated from $\beta = 1.016$, $M_{\max}^{\text{obs}} = 8.8$, and $N[M \geq 6.5] = 66$. The analysis of $M_{\max}$ was repeated, and further modifications to the seismic sources were required (**Fig. 5**).

$$N_C(M_0) = \sum_{M=M_0}^{M_{\max}} \lambda_M \times T_C\left(\boldsymbol{M}_{\max}^{\text{obs}}\right) . \quad . \quad . \quad . \quad . \quad . \quad (5)$$

4.2. $M_{\max}$ for Intraslab Earthquakes

The typically accepted limit of the $M_{\max}$ for intraslab earthquakes is M_{w} 8.0 [20]. Peru's largest documented intraslab earthquake was the 2019 Lagunas Earthquake (M_{w} 8.0) [13]. However, larger intraslab events have been observed in northern Chile (e.g., the M_{w} 8.2 Calama Earthquake in 1950 [30]), and other continents (e.g., the M_{w} 8.3 Okhotsh Earthquake in Russia [31]). Therefore, by using a maximum value of M_{w} 8.2 is reasonable to limit the possible extrapolation of intraslab earthquakes in Peru.

To estimate the $M_{\max}^{\text{K}}$ [14], at recurrence analysis of the zones created considering M_0 equal to M_{w} 5, 5.5, and 6 was performed, and it was verified that n is greater than 50 when $M_{\max}^{\text{K}} - M_0 \approx 2$ and greater than 150 for differences of up to 3 degrees. For zones where this condition was not met, increasingly larger groups were generated until a suitable $N_C(M_0)$ was achieved; for example, the F-4c group was formed by zones F-4c.1 and F-4c.2.

To establish the $M_{\max}^{\text{B}}$, $M_0 = 6$ was considered, from which two models of a priori distributions were constructed: Model I, formed by the a priori distributions of each zone, and Model II, formed only by the a priori distribution of zone F-3c, which was the most unfavorable distribution found. Subsequently, both models were modified based on the likelihood function for each zone (**Fig. 7**). Finally, after determining the average magnitude of each model ($M_{\max}^{\text{BI}}$ and $M_{\max}^{\text{BII}}$), $M_{\max}^{\text{B}}$ was obtained as the mean value because both models report similar results.

To estimate the $M_{\max}^{\text{R-S}}$, the correlations proposed in [20] and a factor referring to the Slab2.0 thickness (W) were used. To estimate this factor, the largest events recorded in the catalog and the maximum W obtained at a radius of 100 km around each event were reviewed. As a result, a reasonable estimate of $M_{\max}^{\text{obs}}$ was found when considering factors of 0.85 and 0.9 with respect to W. When factors close to 0.95 were used, magnitudes greater than M_{w} 8.3 were obtained; therefore, a factor of 0.9 was selected (**Fig. 8**). Finally, $M_{\max}^{\text{R-S}}$ was determined using the 84th percentile of the slab thicknesses included in each zone ($W_{\text{P.84}}$) with a modification factor of 0.9 and the intraslab scaling relationships [20].

To estimate $M_{\max}$ using the empirical increment method ($M_{\max}^{\Delta}$), a Δ of 0.5° was added to $M_{\max}^{\text{obs}}$, but without exceeding the maximum value of M_{w} 8.2.

Table 1 lists the values obtained by all previous approaches and the average value of $M_{\max}$ obtained for each intraslab source.

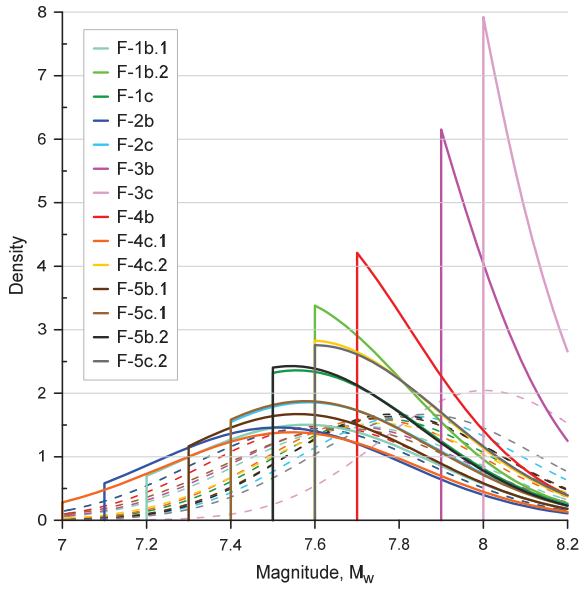

(a)

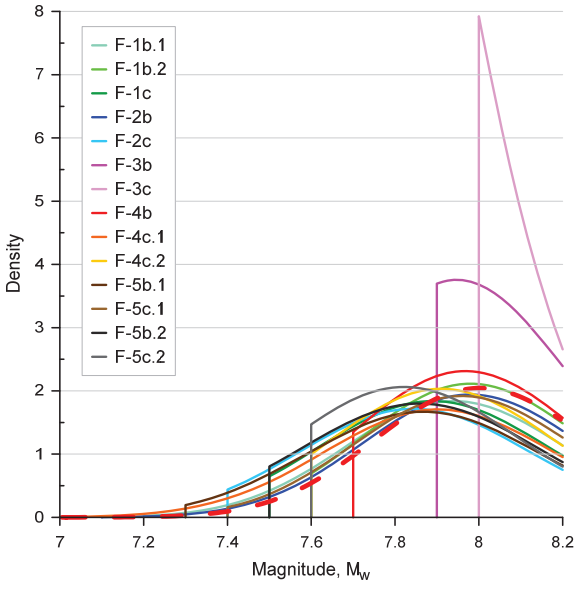

(b)

Fig. 7. A priori (dashed line) and final (solid line) $M_{\max}$ distributions by the Bayesian method (a) Model I and (b) Model II.

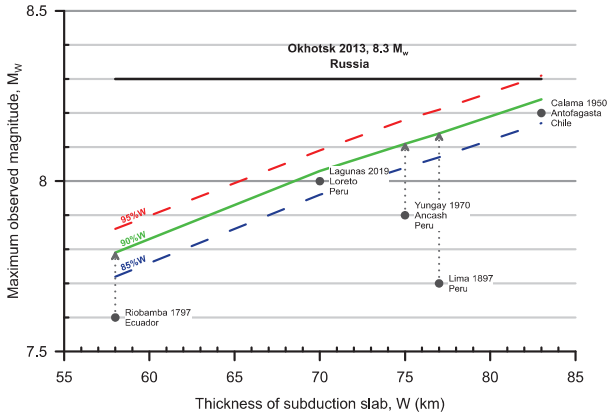

Fig. 8. $M_{\max}^{\mathrm{R-S}}$ estimated for different values of W.

4.3. $M_{\max}$ for Interface Earthquakes

The main characteristic of interface earthquakes in Peru is the heterogeneity of seismic coupling between regions, which can be divided into three regions: north, central, and south [30]. The northern region presents aseismic plate convergence with weak-to-moderate coupling [30]. However, owing to the large uncertainty in the estimation of the momentum deficit, a momentum accumulation of 1,000 years was assigned, which was equivalent to a scenario of M_{w} 8.6–9.0. In the central and southern regions, there are previous studies have used physical models to evaluate historical or extraordinary scenarios. A previous study [8] used hydrodynamic simulations to evaluate tsunami scenarios of the 1868 Arica Earthquake of M_{w} 8.8 and concluded that this event required a rupture greater than M_{w} 9.0 to destroy the city of Pisco. This can only be achieved by extending the rupture across the Nazca Ridge. Likewise, [11, 12] established through interseismic coupling distribution models that the ruptures expected for the central and southern regions of Peru will generate events of M_{w} 8.9 and 8.5, respectively.

Similarly, for the intraslab zonings, to estimate $M_{\max}^{\mathrm{K}}$ [14], a recurrence analysis of the proposed seismic sources was performed considering M_0 equal to M_{w} 6.0 and 7.0. Because an adequate amount of $N_C(M_0)$ was not obtained, two groups were used for evaluation: the northern group (F-1a, F-2a, and F-3a) with $\mathrm{Nc}[\mathrm{M}_0 = 6] = 229$ and the southern group (F-4a and F-5a) with $\mathrm{Nc}[\mathrm{M}_0 = 7] = 55$.

The $M_{\max}^{\mathrm{B}}$ was estimated using a magnitude $M_0 = 7$ and the a priori distributions. Subsequently, using the likelihood function (**Fig. 9**), the value of $M_{\max}^{\mathrm{B}}$ was determined to be the mean magnitude of each distribution.

To estimate the $M_{\max}^{\mathrm{R-S}}$, the highest value obtained from the correlations proposed by Strasser et al. [19] and Allen and Hayes [20] using the rupture area of each source was used. Complementarily, for the $M_{\max}^{\Delta}$ estimation [14] only sources with $M_{\max}^{\mathrm{obs}}$ greater than or equal to M_{w} 8.5 were considered, and a Δ of 0.2 was established.

Table 2 shows the values obtained by all previous approaches and the average value of $M_{\max}$ obtained for each interface source.

5. Discussion of Results

From the analyses, it was determined that the $M_{\max}$ for the seismic sources identified in this study ranges from M_{w} 8.7 to 9.0 for interface sources and from M_{w} 7.6 to 8.1 for intraslab sources. In all cases, these values exceed the $M_{\max}$ values obtained in other regional studies on Peru [2–6]. In particular, for the region delimited by the F-3c intraslab source, where two large-magnitude events (the 1906 earthquake of M_{w} 7.9 and the 2019 Lagunas Earthquake of M_{w} 8.0) occurred, our results estimate an $M_{\max}$ of M_{w} 8.1 ± 0.1, contrasting with the values of M_{w} 7.5 in [2], M_{w} 7.33 in its subsequent update [3], M_{w} 7.5 in [4], M_{w} 7.2 in [5], and M_{w} 7.4 in [6]. It is possible that these values were underestimated due to the occurrence of the Lagunas Earthquake after these studies. However, they still remain 0.4–0.7 magnitude units below the 1906 earthquake of M_{w} 7.9, which is included in the IGP historical seismic catalog but was not considered by these authors.

Similarly, for the F-5a interface source, where the 1868 Arica Earthquake of M_{w} 8.8 occurred, our results estimate an $M_{\max}$ of M_{w} 9.0 ± 0.1. However, other studies assign significantly lower $M_{\max}$ values to this region. Specifically, [2] assigned a value of M_{w} 8.8, [3] assigned M_{w} 8.2, [4] considered M_{w} 8.4, [5] M_{w} 8.8, and [6] M_{w} 8.4. Therefore, the seismic sources proposed in [2–6] need to be updated if included in future studies, preferably by using updated methods for calculating $M_{\max}$ as described in this study. It is unlikely that establishing $M_{\max}$ from $M_{\max}^{\mathrm{obs}}$ will provide an appropriate value for $M_{\max}$; at best, this value will provide a lower bound for $M_{\max}$ [14]. Therefore, other methods must be employed to determine $M_{\max}$.

However, there is a good correlation between our results and those of physical studies on interface sources [10–12]. For example, for the F-5a source, a $M_{\max}$ of M_{w} 9.0 ± 0.1 was established, a value that coincides with that found by Okal et al. [10], which establishes a magnitude greater than M_{w} 9.0 for the 1868 Arica Earthquake. Similarly, Pulido et al. [11] established a magnitude greater than M_{w} 8.5 for the southern region of Peru from the moment deficit. Additionally, in the central region of Peru, for the F-4a source, a $M_{\max}$ of M_{w} 8.9 ± 0.1 was obtained, a value similar to that obtained by Pulido et al. [12], who estimated a magnitude of M_{w} 8.9 for this region based on the moment deficit. Finally, for F-2a and F-3a sources, a $M_{\max}$ of M_{w} 8.7 to 8.8 ± 0.1 was established in the northern region of Peru. Villegas-Lanza et al. [32], considering the moment deficit in this region, estimated a magnitude between M_{w} 6.6 and 7.0; however, given the high uncertainty in the moment deficit rate, he extrapolated to 1,000 years and obtained a magnitude of M_{w} 8.6 to 9.0 for the expected event. Consequently, given the uncertainty associated with this region, it is reasonable to use the values obtained in this study.

Table 1. M_{max} estimation for intraslab sources.

Source	M_{max}^{obs}	Group	$N_C(M_0)$[a]	M_{max}^{K}[b]	M_{max}^{BI}	M_{max}^{BII}	M_{max}^{B}[c]	$W_{P.84}$[d]	M_{max}^{R-Se}	M_{max}[f]
F-1b.1	7.3	F-1b, F-1c, F-2b, and F-2c	72	7.7	7.6	7.9	7.7	51.8	7.7	7.7
F-1b.2	7.6		72	7.7	7.8	7.9	7.9	59.7	7.8	7.9 ± 0.2
F-1c	7.5		72	7.7	7.7	7.9	7.8	57.6	7.8	7.8 ± 0.1
F-2b	7.1		72	7.7	7.6	7.9	7.7	64.8	7.9	7.7 ± 0.1
F-2c	7.4		72	7.7	7.7	7.8	7.8	64.0	7.9	7.8 ± 0.1
F-3b	7.9	All intraslab sources	230	8.1	8.0	8.0	8.0	70.0	8	8.1 ± 0.1
F-3c	8		230	8.1	8.1	8.1	8.1	70.7	8	8.1 ± 0.1
F-4b	7.7	F-4b and F-4c	2,045*	7.8	7.9	8.0	7.9	77.4	8.2	8.0 ± 0.2
F-4c.1	7	F-4c.1	91	7.2	7.6	7.8	7.7	75.7	8.1	7.6 ± 0.4
F-4c.2	7.6	F-4c	1,420*	7.7	7.8	7.9	7.9	77.9	8.2	8.0 ± 0.2
F-5b.1	7.3	F-5b.1	700	7.5	7.6	7.8	7.7	79.6	8.2	7.8 ± 0.3
F-5c.1	7.4	F-5b.1 and F-5c.1	827*	7.6	7.7	7.9	7.8	79.9	8.2	7.9 ± 0.3
F-5b.2	7.5	F-5b.2	926*	7.7	7.7	7.9	7.8	85.3	8.2	7.9 ± 0.2
F-5c.2	7.6	F-5b.2 and F-5c.2	50	7.8	7.8	7.9	7.8	85.3	8.2	8.0 ± 0.2

a. Number of events corrected for magnitudes greater than M_0 up to $\Delta_M = 2$ and "*" for $\Delta_M = 3$.
b. Estimating M_{max} for intraslab sources using Kijko's method [16].
c. Estimating M_{max} for intraslab sources using the Bayesian method.
d. Estimating M_{max} for intraslab sources from scaling relations.
e. $W_{P.84}$ is the 84th percentile of rupture widths in km.
f. M_{max} values are the average maximum magnitude and its deviation, considering M_{max}^{Δ}, M_{max}^{K}, M_{max}^{B}, and M_{max}^{R-S}.

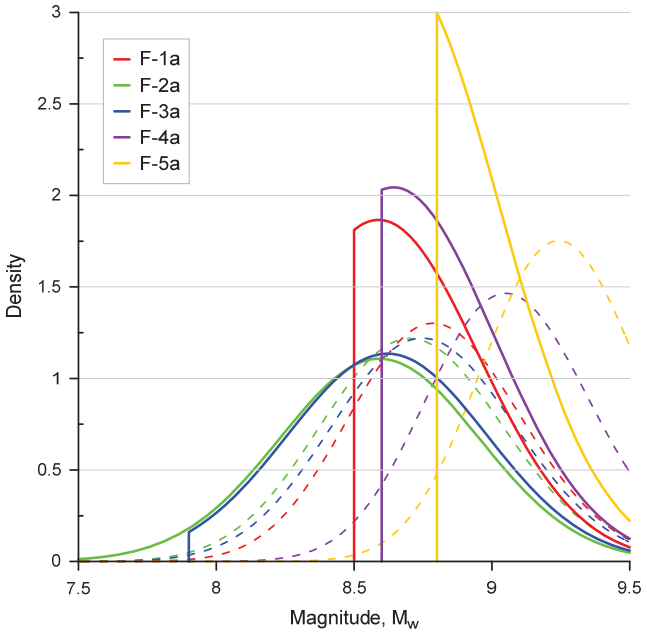

Fig. 9. M_{max} distributions by the Bayesian method for interface sources.

Table 2. Estimation of M_{max} for interface sources.

Source	M_{max}^{obs}	M_{max}^{K}[a]	M_{max}^{B}[b]	M_{max}^{R-Sc}	M_{max}[d]
F-1a	8.5	8.7	8.8	8.8	8.8 ± 0.1
F-2a	7.3	8.7	8.7	8.8	8.7 ± 0.1
F-3a	7.9	8.7	8.7	8.9	8.8 ± 0.1
F-4a	8.6	8.9	8.7	9.0	8.9 ± 0.1
F-5a	8.8	8.9	9.0	9.0	9.0 ± 0.1

a. Estimating M_{max} for intraslab sources using Kijko's method [16].
b. Estimating M_{max} for intraslab sources using the Bayesian method.
c. Estimating M_{max} for intraslab sources from scaling relations.
d. M_{max} are the average maximum magnitude and its deviation, considering M_{max}^{Δ}, M_{max}^{K}, M_{max}^{B}, and M_{max}^{R-S}.

6. Conclusions

To determine the M_{max} associated with each region of Peru, seismic zonation was first performed using Kijko's method [16] and the present tectonic settings to derive 19 subduction seismic source. For each seismogenic sources, the M_{max} was determined as the average of the values estimated using four different methods. The M_{max} established in this study ranges from M_w 8.7 to 9.0 for the interface sources and M_w 7.6 to 8.1 for the intraslab sources. From the comparisons made with the estimates of M_{max} considered in previous studies [2–6], it was found that the results of this study are more conservative and consistent with the historical and instrumental seismicity available. Therefore, the regional maps of estimated seismic [2–6] demands parameters for Peru need to be updated. In conclusion, we recommend updating this study whenever larger M_{max}^{obs} values occur in the region.

Acknowledgments

This study was conducted under the Science and Technology Research Partnership for Sustainable Development (SATREPS) project of the Japan Peru Center for Earthquake Engineering Research and Disaster Mitigation (CISMID). Special thanks to the company, ZER Geosystem Perú, for providing the database used in this research, and to Luis Sandoval for his help with data processing.

References:

[1] J. Baker, B. Bradley, and P. Stafford, "Seismic Hazard and Risk Analysis," Cambridge University Press, 2021. https://doi.org/10.1017/9781108425056

[2] J. L. Castillo Aedo and J. E. Alva Hurtado, "Seismic Hazard in Peru," Bachelor's Thesis, School of Civil Engineering, National University of Engineering, 1994 (in Spanish).

[3] A. M. Bolaños Luna and O. M. Monroy Concha, "Uniform Seismic Hazard Spectra," Master's Thesis, Faculty of Science and Engineering, Pontifical Catholic University of Peru, 2004 (in Spanish).

[4] C. A. Gamarra Rivera and Z. Aguilar Bardales, "New seismogenic sources for seismic hazard assessment and generation of uniform hazard spectra in Peru," Bachelor's Thesis, School of Civil Engineering, National University of Engineering, 2009 (in Spanish).

[5] H. Tavera et al., "Re-evaluation of the probabilistic seismic hazard for Peru," Geophysical Institute of Peru, 2014 (in Spanish). http://hdl.handle.net/20.500.12816/783 [Accessed November 30, 2022]

[6] M. Á. Roncal Castro and Z. Aguilar Bardales, "Determination of the seismic hazard in the national territory and development of a web application," Bachelor's Thesis, School of Civil Engineering, National University of Engineering, 2017 (in Spanish).

[7] E. S. Ferro, "Historia de los sismos más notables ocurridos en el Perú (1513-1974)," Boletín No.3, Serie C: Geodinámica e Ingeniería Geológica, Instituto de Geología y Minería, 1978 (in Spanish). https://hdl.handle.net/20.500.12544/251 [Accessed November 30, 2022]

[8] S. L. Beck and L. J. Ruff, "Great earthquakes and subduction along the Peru trench," Phys. Earth Planet. Inter., Vol.57, Nos.3-4, pp. 199-224, 1989. https://doi.org/10.1016/0031-9201(89)90112-X

[9] L. Dorbath, A. Cisternas, and C. Dorbath, "Assessment of the size of large and great historical earthquakes in Peru," Bull. Seismol. Soc. Am., Vol.80, No.3, pp. 551-576, 1990. https://doi.org/10.1785/BSSA0800030551

[10] E. A. Okal, J. C. Borrero, and C. E. Synolakis, "Evaluation of tsunami risk from regional earthquakes at Pisco, Peru," Bull. Seismol. Soc. Am., Vol.96, No.5, pp. 1634-1648, 2006. https://doi.org/10.1785/0120050158

[11] N. Pulido et al., "Estimation of a source model and strong motion simulation for Tacna City, South Peru," J. Disaster Res., Vol.9, No.6, pp. 925-930, 2014. https://doi.org/10.20965/jdr.2014.p0925

[12] N. Pulido et al., "Scenario source models and strong ground motion for future mega-earthquakes: Application to Lima, Central Peru," Bull. Seismol. Soc. Am., Vol.105, No.1, pp. 368-386, 2015. https://doi.org/10.1785/0120140098

[13] H. Tavera, "May 26, 2019 Lagunas earthquake (M8.0): Seismological aspects," Geological, Mining and Metallurgical Institute, 2019 (in Spanish). http://hdl.handle.net/20.500.12816/4846 [Accessed November 30, 2022]

[14] R. L. Wheeler, "Methods of Mmax Estimation East of the Rocky Mountains," Open-File Report 2009-1018, United Status Geological Survey, 2009. https://doi.org/10.3133/ofr20091018

[15] A. Kijko and M. A. Sellevoll, "Estimation of earthquake hazard parameters from incomplete data files. Part I. Utilization of extreme and complete catalogs with different threshold magnitudes," Bull. Seismol. Soc. Am., Vol.79, No.3, pp. 645-654, 1989. https://doi.org/10.1785/BSSA0790030645

[16] A. Kijko, "Estimation of the maximum earthquake magnitude, $m_{\max}$," Pure Appl. Geophys., Vol.161, No.8, pp. 1655-1681, 2004. https://doi.org/10.1007/s00024-004-2531-4

[17] A. C. Johnston, K. J. Coppersmith, L. R. Kanter, and C. A. Cornell, "The Earthquakes of Stable Continental Regions: Vol.1: Assessment of Large Earthquake Potential," TR-102261-V1, Electric Power Research Institute, 1994.

[18] "Technical Report: Central and Eastern United States Seismic Source Characterization for Nuclear Facilities," U.S. Nuclear Regulatory Commission, U.S. Department of Energy, and Electric Power Research Institute, 2012.

[19] F. O. Strasser, M. C. Arango, and J. J. Bommer, "Scaling of the source dimensions of interface and intraslab subduction-zone earthquakes with moment magnitude," Seismol. Res. Lett., Vol.81, No.6, pp. 941-950, 2010. https://doi.org/10.1785/gssrl.81.6.941

[20] T. I. Allen and G. P. Hayes, "Alternative rupture-scaling relationships for subduction interface and other offshore environments," Bull. Seismol. Soc. Am., Vol.107, No.3, pp. 1240-1253, 2017. https://doi.org/10.1785/0120160255

[21] E. M. Scordilis, "Empirical global relations converting $\mathbf{M}_S$ and $\mathbf{m}_b$ to moment magnitude," J. Seismol., Vol.10, No.2, pp. 225-236, 2006. https://doi.org/10.1007/s10950-006-9012-4

[22] M. Pagani, K. Johnson, and J. G. Pelaez, "Modelling subduction sources for probabilistic seismic hazard analysis," Geol. Soc. Lond. Spec. Publ., Vol.501, pp. 225-244, 2020. https://doi.org/10.1144/SP501-2019-120

[23] G. P. Hayes et al., "Slab2, a comprehensive subduction zone geometry model," Science, Vol.362, No.6410, pp. 58-61, 2018. https://doi.org/10.1126/science.aat4723

[24] M. E. Pasyanos, T. G. Masters, G. Laske, and Z. Ma, "LITHO1.0: An updated crust and lithospheric model of the Earth," J. Geophys. Res. Solid Earth, Vol.119, No.3, pp. 2153-2173, 2014. https://doi.org/10.1002/2013JB010626

[25] G. Ekström, M. Nettles, and A. M. Dziewoński, "The global CMT project 2004–2010: Centroid-moment tensors for 13,017 earthquakes," Phys. Earth Planet. Inter., Vols.200-201, pp. 1-9, 2012. https://doi.org/10.1016/j.pepi.2012.04.002

[26] J. K. Gardner and L. Knopoff, "Is the sequence of earthquakes in Southern California, with aftershocks removed, Poissonian?," Bull. Seismol. Soc. Am., Vol.64, No.5, pp. 1363-1367, 1974. https://doi.org/10.1785/BSSA0640051363

[27] R. A. Uhrhammer, "Characteristics of northern and central California seismicity," Earthq. Notes, Vol.57, No.1, pp. 21-37, 1986.

[28] J. C. Stepp, "Analysis of completeness of the earthquake sample in the Puget Sound area and its effect on statistical estimates of earthquake hazard," Proc. of the Int. Conf. on Microzonazion for Safer Construction Research and Application, Vol.2, pp. 897-910, 1972.

[29] G. Ameri et al., "On the choice of maximum earthquake magnitude for seismic hazard assessment in metropolitan France – Insight from the Bayesian approach," 9ème Colloque National AFPS, 2015.

[30] National Library of Chile, "Los terremotos en Chile (1570-2010)," Chilean Memory (in Spanish). https://www.memoriachilena.gob.cl/602/w3-article-3576.html [Accessed July 12, 2022]

[31] L. Ye, T. Lay, H. Kanamori, and K. D. Koper, "Energy release of the 2013 M_w 8.3 Sea of Okhotsk earthquake and deep slab stress heterogeneity," Science, Vol.341, No.6152, pp. 1380-1384, 2013. https://doi.org/10.1126/science.1242032

[32] J. C. Villegas-Lanza et al., "Active tectonics of Peru: Heterogeneous interseismic coupling along the Nazca megathrust, rigid motion of the Peruvian Sliver, and Subandean shortening accommodation," J. Geophys. Res. Solid Earth, Vol.121, No.10, pp. 7371-7394, 2016. https://doi.org/10.1002/2016JB013080

Name:
Juan Carlos Tarazona

ORCID:
0000-0002-3761-2700

Affiliation:
Research Assistant, Japan Peru Center for Earthquake Engineering Research and Disaster Mitigation (CISMID), National University of Engineering (UNI)

Address:
Av. Tupac Amaru 1150, Lima 15333, Peru

Brief Career:
2018- ZER Geosystem Perú
2020- Research Assistant, CISMID, UNI
2022- Seismic Hazards Committee, Seismic Model Code for Latin America and the Caribbean (CMS)

Selected Publications:
• "Site response analysis and its comparison with the Peruvian seismic design spectrum," Tecnia, Vol.29, No.2, pp. 91-97, 2019.
• "Dynamic analysis of a highway cut and cover tunnel in Lima City, Peru," Proc. of the 17th World Conf. on Earthquake Engineering (17WCEE), C003608, 2020.

Academic Societies & Scientific Organizations:
• Committee of the Seismic Model Code for Latin America and the Caribbean (CMS), Seismic Hazards Committee

Name:
Zenon Aguilar

ORCID:
0000-0003-4710-3333

Affiliation:
Professor, Japan Peru Center for Earthquake Engineering and Disaster Mitigation (CISMID), Faculty of Civil Engineering, National University of Engineering (UNI)

Address:
Av. Tupac Amaru 1150, Lima 15333, Peru

Brief Career:
1982-1988 UNI
1993-1999 Kyoto University
1999-2017 Associate Professor, UNI
2018- Professor, UNI

Selected Publications:
• "Peruvian subduction surface model for seismic hazard assessments," Civ. Eng. J., Vol.5, No.5, pp. 984-995, 2019.
• "Scenario source models and strong ground motion for future mega-earthquakes: Application to Lima, central Peru," Bull. Seismol. Soc. Am., Vol.105, No.1, pp. 368-386, 2015.
• "Evaluation of surface soil amplification for wide areas in Lima, Peru," J. Disaster Res., Vol.8, No.2, pp. 259-265, 2013.

Academic Societies & Scientific Organizations:
• Peruvian Engineers Association (CIP)
• Peruvian Association of Geotechnical Engineering (APGEO)
• American Society of Civil Engineers (ASCE)

Name:
Nelson Pulido

Affiliation:
Senior Researcher, National Research Institute for Earth Science and Disaster Resilience (NIED)

Address:
3-1 Tennodai, Tsukuba, Ibaraki 305-0006, Japan

Brief Career:
1990 Received Bachelor degree from Universidad de los Andes
1992 Received Master's degree of Engineering from Universidad de los Andes
1993-1996 Researcher, Colombian Geological Survey
2000 Ph.D. degree in Science from Kyoto University
2000-2001 Research Fellow, RIKEN
2001- NIED

Selected Publications:
• "Broadband wavelength slip model of the 1906 Ecuador-Colombia megathrust-earthquake based on seismic intensity and tsunami data," Tectonophysics, Vol.774, 228226, 2020. https://doi.org/10.1016/j.tecto.2019.228226
• "Scenario source models and strong ground motion for future mega-earthquakes: Application to Lima, Central Peru," Bull. Seismol. Soc. Am., Vol.105, No.1, pp. 368-386, 2015.
• "Estimation of the high-frequency radiation of the 2000 Tottori (Japan) earthquake based on a dynamic model of fault rupture: Application to the strong ground motion simulation," Bull. Seismol. Soc. Am., Vol.99, No.4, pp. 2305-2322, 2009.

Academic Societies & Scientific Organizations:
• American Geophysical Union (AGU)
• Japan Geosciences Union (JpGU)
• The Seismological Society of Japan (SSJ)

Name:
Carlos Gonzales

ORCID:
0000-0002-8940-2086

Affiliation:
Researcher, Japan Peru Center for Earthquake Engineering Research and Disaster Mitigation (CISMID), Faculty of Civil Engineering, National University of Engineering (UNI)

Address:
Av. Tupac Amaru 1150, Lima 15333, Peru

Brief Career:
2009 Received B.S. degree in Civil Engineering from UNI
2014 Received M.Eng. degree from Chiba University
2017 Received Ph.D. degree from Chiba University

Selected Publications:
• "Site dominant frequencies in Lima, Peru, by H/V spectral ratio of seismic records," Tecnia, Vol.32, No.2, pp. 171-184, 2022.
• "Evaluation of the seismic response using random vibration theory in three soil profiles of Lima, Peru," Tecnia, Vol.32, No.2, pp. 89-100, 2022.

Academic Societies & Scientific Organizations:
• Seismological Society of America (SSA)
• Earthquake Engineering Research Institute (EERI)

Name:
Fernando Lazares

ORCID:
0000-0002-9945-412X

Affiliation:
Professor, Faculty of Civil Engineering, National University of Engineering (UNI)

Address:
Av. Tupac Amaru 1150, Lima 15333, Peru

Brief Career:
2003 Received Master's degree from National Autonomous University of Mexico
2003- Professor, UNI

Selected Publications:
• "Evaluation of surface soil amplification for wide areas in Lima, Peru," J. Disaster Res., Vol.8, No.2, pp. 259-265, 2013.

Name:
Hiroe Miyake

Affiliation:
Associate Professor, Earthquake Research Institute, The University of Tokyo

Address:
1-1-1 Yayoi, Bunkyo-ku, Tokyo 113-0032, Japan

Brief Career:
2005- Assistant Professor, The University of Tokyo
2015- Associate Professor, The University of Tokyo

Selected Publications:
• "Source fault of the 2007 Chuetsu-oki, Japan, earthquake," Bull. Seismol. Soc. Am., Vol.100, No.1, pp. 384-391, 2010.
• "Special issue 'The 2015 Gorkha, Nepal, earthquake and Himalayan studies: First results'," Earth Planets Space, Vol.69, No.1, 12, 2017.
• "Characterized source modeling of crustal earthquakes for broadband ground motion prediction," International Atomic Energy Agency (IAEA), "Best Practices in Physics Based Fault Rupture Models for Seismic Hazard Assessment of Nuclear Installations," IAEA-TECDOC-CD-1833, pp. 270-276, 2018.

Academic Societies & Scientific Organizations:
• American Geophysical Union (AGU)
• Seismological Society of America (SSA)
• The Seismological Society of Japan (SSJ)